horticulturae

MDPI

Article

Genome-Wide Analysis of B-Box (BBX) Gene Family in Red Walnut (*Juglans regia* L.) and *JrBBX3* Function in Relation to Anthocyanin Biosynthesis

Junru Chen [1,†], Manyao Guo [1,†], Susu Tie [1], Xiaobei Wang [1,2], Haipeng Zhang [1,2], Xiaodong Lian [1,2], Nan Hou [1,2], Jiancan Feng [1,2], Lei Wang [1,2,*] and Bin Tan [1,2,*]

[1] College of Horticulture, Henan Agricultural University, Zhengzhou 450046, China; chenjunru2026@163.com (J.C.); guomanyao2027@163.com (M.G.); tiesusu@163.com (S.T.); wangxb@henau.edu.cn (X.W.); haipengzhang@henau.edu.cn (H.Z.); lianxd@henau.edu.cn (X.L.); nanhou@henau.edu.cn (N.H.); jcfeng@henau.edu.cn (J.F.)
[2] Henan Key Laboratory of Fruit and Cucurbit Biology, Zhengzhou 450046, China
* Correspondence: wanglei2017@henau.edu.cn (L.W.); btan@henau.edu.cn (B.T.)
† These authors contributed equally to this work.

Abstract

Walnut is an important nut with a rich nutritional profile and associated health benefits for the human body. B-box (BBX) proteins containing one or two BBX motifs play pivotal roles in plant growth and developmental processes; nevertheless, the functions of *JrBBXs* in walnut anthocyanin biosynthesis remain inadequately understood. In this study, 39 *JrBBXs* in red walnut 'RW-1' were identified, with phylogenetic analysis suggesting that they were divided into six classes based on the distribution of conserved domains and unevenly distributed on 14 chromosomes. Promoter analysis demonstrated that *JrBBX* promoters possessed an abundance of light responsiveness elements, ABA responsiveness elements, MYB binding sites and MYC binding sites. The transcriptome analysis results demonstrated that eight *JrBBXs* were differently expressed in normal green walnut 'Zhonglin 1' and red walnut 'RW-1' seed coats. Furthermore, qRT-PCR (quantitative real-time polymerase chain reaction) analysis showed that *JrBBX3* exhibited lower expression during seed coat development in 'RW-1'. Y1H (Yeast One-Hybrid) and LUC (dual-luciferase reporter) assays revealed that JrBBX3 directly inhibited the expression of *JrUFGT5*, considered a key anthocyanin biosynthesis structural gene in research. Subcellular localization analysis indicated both cytoplasmic and nuclear localization of JrBBX3. Transient overexpression of *JrBBX3* in walnut leaves resulted in reduced *JrUFGT5* expression and anthocyanin accumulation. Collectively, these findings revealed the negative regulation of JrBBX3 in red walnut anthocyanin biosynthesis, and provided a basis to further study the anthocyanin biosynthesis mechanism of red walnut.

Keywords: BBX transcription factor; expression pattern; gene function; *cis*-acting element; walnut seed coat

Check for updates

Academic Editor: Radu E. Sestras

Received: 25 March 2026
Revised: 18 April 2026
Accepted: 20 April 2026
Published: 22 April 2026

Copyright: © 2026 by the authors. Licensee MDPI, Basel, Switzerland. This article is an open access article distributed under the terms and conditions of the Creative Commons Attribution (CC BY) license.

1. Introduction

Anthocyanins are water-soluble natural pigments responsible for the diverse colors in plant organs, including stems, leaves, flowers, fruits, and seeds [1], and play crucial ecological roles in various plant stress resistance reactions [2]. Their biosynthetic pathway involves multiple enzymes and intermediate metabolites: First, phenylalanine deaminase

(PAL), as the initiating enzyme in anthocyanin biosynthesis, converts phenylalanine into cinnamic acid [3]. Subsequently, cinnamic acid-4-hydroxylase (C4H) and 4-coumaroyl-CoA ligase (4CL) catalyze the formation of coumaroyl-CoA [4], which is converted into chalcone under chalcone synthase (CHS) catalysis [5]. Chalcone isomerase (CHI) catalyzes the formation of naringin from chalcone, while flavanone 3-hydroxylase (F3H) flavonoid 3′-hydroxylase (F3′H) and flavonoid 3′,5′-hydroxylase (F3′5′H) hydroxylate naringin to generate dihydroflavonol, which is further catalyzed by dihydroflavonol 4-reductase (DFR) and anthocyanidin synthase (ANS) to generate colored anthocyanidins [6], and UDP-glucosylflavone-3-*O*-glycosyltransferase (UFGT) catalyzes glycosylation to form stable anthocyanins [7]. The expressions of these structural genes are primarily regulated by the MYB, bHLH, and WD40 transcription factors (TFs), which often act synergistically through the formation of the MBW complex (MYB/bHLH/WD40) [8–11].

Beyond the well-reported MBW complex, additional TFs also play roles in regulating anthocyanin biosynthesis. B-box (BBX) proteins, characterized by one or two B-box zinc finger domains, constitute one such group that are phylogenetically classified into five structural classes (I–V) based on their domain composition (B-box, CCT, VP): class I contains two B-box domains, one CCT-domain (CONSTANS, CO-LIKE and TOC1 motif), and VP (valine-proline) motif; class II contains two B-box domains and one CCT domain; class III contains one B-box domain and one CCT domain; class IV contains two B-box domains; and class V contains only one B-box domain [12]. BBX proteins act as central regulators in light signal transduction, pigment accumulation, and abiotic stresses.

Regarding light stress, BBXs interact directly with core light signaling components, such as HY5 and COP1, to balance photosynthetic efficiency and photoprotection. Several BBX proteins in Arabidopsis, including BBX4, BBX11, BBX20, BBX21, BBX22, and BBX23 promote photomorphogenesis [13–15], while other BBX proteins in Arabidopsis, such as BBX18, BBX19, BBX24, BBX25, BBX28, BBX29, BBX30, BBX31, and BBX32, repress photomorphogenesis [16]. OsBBX14 promoted the expression of *OsHY5L1* to enhance photomorphogenesis in rice under blue-light conditions [17], and seven *CeBBX* genes in *Cymbidium ensifolium* showed a direct response to blue-light signaling [18]. Phylogenetic tree analysis of chestnuts revealed that the first class CmBBX may be involved in photomorphogenesis and flowering processes in chestnut species [19]. Notably, *BBX* genes served as molecular hubs in the crosstalk between light signaling and anthocyanin biosynthesis. In *Arabidopsis thaliana*, AtBBX21 and AtBBX22 interacted with HY5 to promote anthocyanin biosynthesis [20,21], while AtBBX23 positively regulated *CHS* expression [22]. Conversely, AtBBX24, AtBBX25 and AtBBX32 acted as negative regulators [23–25]. In red pear (*Pyrus pyrifolia*), PpBBX18 and PpBBX21 antagonistically regulated anthocyanin biosynthesis via interaction with PpHY5 [26]; PpBBX16 directly bound the promoter of *MYB10* to positive anthocyanin biosynthesis [27], and *PyBBX24* (*Pyrus* spp.) had no effect, but its allelic variation, termed $PyBBX24^{\Delta N14}$, was conducive to the biosynthesis of anthocyanins [28]. In apple (*Malus domestica*), MdBBX37 suppressed biosynthesis by down-regulating *MdMYB1*, *MdMYB9*, and *MdHY5* [29]. In grape (*Vitis vinifera*), VvBBX8 and VvBBX11 interacted with VvBBX32 to activate *VvBZR1* expression, enhancing anthocyanin biosynthesis [30].

Walnut (*Juglans regia* L.) is one of the four major dried fruits worldwide. Walnut kernels are rich in diverse nutrients, primarily including: fatty acids (60–70%), dominated by unsaturated fatty acids such as oleic acid, linoleic acid, and linolenic acid; proteins (15–20%), including eight essential amino acids (valine, threonine, leucine, isoleucine, methionine, phenylalanine, lysine and tryptophan) required by the human body; and vitamins (notably vitamin E 26 mg/100 g) [31]. Epidemiological investigations and clinical trials have demonstrated that regular walnut intake significantly lowered the incidence of

cardiovascular diseases (CVDs), including coronary artery disease and ischemic stroke [32]. As one of the origins of walnut, China has a long history of walnut cultivation. According to the FAO (the Food and Agriculture Organization of the United Nations) database (https://www.fao.org/faostat/zh/#data/QCL/visualize, accessed on 18 April 2026), the walnut harvest area in China is 371,689 ha, producing of 1.15 million tons and ranking first in the world in terms of both harvest area and yield. At present, the main walnut varieties cultivated in China have green leaves and peels, and a light-yellow seed coat. However, the unique wild resource 'RW-1' exhibits red pigmentation in its leaves, peels, and seed coat due to anthocyanin accumulation, and mainly Cyanidin-3-*O*-Galactoside in red walnut leaves and Delphinidin-3-*O*-Glucoside in red walnut fruit peels [33]. Although many key genes (e.g., *JrbHLHs*, *JrUFGT5*) involved in anthocyanin biosynthesis have been characterized [34–36], the specific regulatory functions of *BBX* genes in walnut anthocyanin biosynthesis remain uncharacterized.

In this study, walnut *BBX* gene members were identified, and their physicochemical properties, phylogenesis, chromosome location, gene structure, *cis*-acting elements (CAEs), conserved motifs, gene replication, and protein–protein interactions were comprehensively analyzed. Given the critical roles of BBXs in anthocyanin biosynthesis, this study further examined the function of JrBBX3. This integrated approach provided foundational insights into the potential regulatory mechanisms of JrBBX proteins governing anthocyanin biosynthesis in red walnut, addressing a significant gap in knowledge.

2. Materials and Methods

2.1. Plant Materials

Common walnut (*J. regia* L. 'Zhonglin 1') and wild resource red walnut (*J. regia* L. accession 'RW-1') test cultivar materials were all cultivated at the Fruit Tree Germplasm Experimental Station of College of Horticulture, Henan Agricultural University (113°35′ E, 34°58′ N, Zhengzhou, China). Seed coats from the two walnut types were harvested at three key development stages: S1 (fruit shell hardening stage, 60 days after female flowering, 25 June 2025), S2 (seed kernel filling stage, 90 days after female flowering, 25 July 2025) and S3 (fruit ripening stage, 120 days after female flowering, 24 August 2025). All the samples were immediately flash-frozen in liquid nitrogen and stored at −80 °C.

The tobacco (*Nicotiana benthamiana*) seeds stored in the laboratory were sprinkled on the moist substrate. After being maintained in a temperature incubator at 25 °C and a 16 h day/8 h night photoperiod for four weeks, the plants were used for Luciferase complementation assay and subcellular localization.

2.2. Identification of the BBX Family Genes in Walnut

Walnut protein sequence datasets (*J. regia* Genome V1.0) were downloaded from the Juglans Genome Projects (http://xhhuanglab.cn/data/juglans.html, accessed on 18 April 2026) [37]. Known *Arabidopsis thaliana* BBX protein sequences served as queries for BLASTP searches against the walnut dataset using TBtools (v2.446) [38]. Hidden Markov Model (HMM) profiles for the BBX domain (Pfam accession: PF00643) were retrieved from the Pfam database (https://www.ebi.ac.uk/interpro/entry/pfam/, accessed on 18 April 2026) [39], and used to identify candidate *JrBBX* genes via HMMER v 3.1 (E-value $\leq 1 \times 10^{-5}$).

2.3. Physicochemical Characterization, Secondary Structures and Three-Dimensional Structures of JrBBX Proteins

The physicochemical characterization (including CDS length, amino acid count, molecular weight (MW, kDa), and isoelectric point (pI)) and subcellular localization of JrBBX proteins were predicted by submitting the protein sequences to ExPASy ProtParam

(https://web.expasy.org/protparam/, accessed on 18 April 2026) [40] and WoLF PSORT (https://wolfpsort.hgc.jp/, accessed on 18 April 2026) [41] respectively. Chromosome localizations were mapped using 'Gene Location Visualze from GTF/GFF' in TBtools (v2.446) [41].

Secondary structures of JrBBX proteins were predicted using SOPMA (https://npsa-prabi.ibcp.fr/cgi-bin/npsa_automat.pl?page=/NPSA/npsa_sopma_f.html, accessed on 18 April 2026) with four conformational states, and then statistical analyses of α-helices, extended strands, β-turns, and random coils were performed. Three-dimensional structures were modeled by submitting protein sequences to SWISS-MODEL (https://swissmodel.expasy.org/interactive, accessed on 18 April 2026), and the generated Protein Data Bank (PDB) files were used to visualize the secondary structure elements within the 3D conformations of these proteins via the PyMOL(3.0.3) software [42,43].

2.4. Conserved Motifs, Multiple Sequences Phylogenetic, and Collinearity Analyses of JrBBXs

Conserved domains of JrBBX protein sequences were predicted using NCBI-CDD (https://www.ncbi.nlm.nih.gov/cdd/, accessed on 18 April 2026), the generated ASN Text files were visualized using 'Visualize Domain Pattern (from NCBI Batch-CDD)' in Tbtools (v2.446) [38]. JrBBX conserved motifs were predicted on the MEME website (http://meme-suite.org/tools/meme, accessed on 18 April 2026), and the generated MAST XML output was visualized using 'Visualize Motif Pattern (from meme.xml/mast.xml (MEME suite))' of Tbtools (v2.446) [44]. The analysis of the *JrBBX* gene structures was conducted using 'Redraw Gene structure (from GTF/GFF3 File)' in Tbtools (v2.446) [38]. A phylogenetic tree was constructed using the MEGA11 software, aligning JrBBX proteins with Arabidopsis BBXs (Table S2) and anthocyanin biosynthesis-related BBX proteins from other species via the Maximum Likelihood method with 1000 bootstrap replicates. The Jones–Taylor–Thornton (JTT) model was used to determine uniform rates among samples. The ML Heuristic Method was Nearest-Neighbor Interchange (NNI) and the initial tree for ML was made automatically (Default—NJ/BioNJ) [45]. The protein sequences used in this article were listed in Table S3.

For collinearity, the genome sequence of *Arabidopsis thaliana* was downloaded from Ensembl Plants (https://plants.ensembl.org/index.html, accessed on 18 April 2026), and that of *J. sigillata* was downloaded from the Juglans Genome Projects (http://xhhuanglab.cn/data/juglans.html, accessed on 18 April 2026). For the intra-family collinearity of the *JrBBX* gene family, the homology between *J. regia* and *Arabidopsis thaliana*, *J. sigillata* were analyzed using 'MCScanX' and visualized using 'Advanced Circos' of TBtools (v2.446) [46].

2.5. Prediction of JrBBX Protein–Protein Interactions, and Promoter Key Cis-Element Analysis of JrBBX Family Genes

Protein–protein interaction networks were predicted using the STRING database (https://cn.string-db.org/, accessed on 18 April 2026) with Arabidopsis as a reference organism (minimum required interaction score of 0.4); the generated TSV files were visualized using Cytoscape v3.10.1 software.

Putative promoter regions (2000 bp upstream of the ATG start codon) were extracted with TBtools (v2.446). The key *cis*-elements were identified using PlantCARE (https://bioinformatics.psb.ugent.be/webtools/plantcare/html/, accessed on 18 April 2026), and the results were then visualized using 'Simple BioSequence Viewer' in TBtools (v2.446) [47].

2.6. Expression Pattern Analysis of JrBBX Genes in Walnut Seed Coat and qRT-PCR Analysis

RNA-seq data (PRJNA1405992) generated from seed coats at different developmental stages were used to analyze *JrBBX* expression trends. Gene expression levels were estimated by FKPM (fragments per kilobase of transcript per million fragments mapped).

Three biological replicates were performed for each sample. Genes with $|\log_2 FC| \geq 1$ and FDR < 0.05 were considered differentially expressed, and the analysis was conducted using DESeq2 (1.30.1).

Total RNA of different seed coats was extracted using the FastPure Universal PlantTotal RNA Isolation Kit (Vazyme, Nanjing, China). First-strand cDNA was synthesized using the EX RT Kit (gDNA remover) (Zoman, Beijing, China). Reverse transcription quantitative PCR (qRT-PCR) was performed using the SYBR Green Premix SupTag HS qPCR Kit (Accurate, Shanghai, China) on an ABI 7500 Real-Time PCR system (Applied Biosystems, Foster City, CA, USA). The walnut *18S* rRNA gene served as the internal control. Relative gene expression levels were calculated using the $2^{-\Delta\Delta Ct}$ method. All the primers used in this study are shown in Table S1.

2.7. Subcellular Localization of JrBBX3

The CDS of *JrBBX3* was amplified from 'RW-1' cDNA and subsequently cloned into the pCAMBIA2300-GFP vector to construct the recombinant plasmid 35S-JrBBX3-GFP, and 35S-GFP served as the control. All constructs were transformed into *Agrobacterium tumefaciens* strain GV3101, and resuspended in a MES suspension solution (B&M, Beijing, China) to OD_{600} = 0.6–0.8. After culturing in the dark for 3 h, the resuspended solution was injected into the leaves of four-week-old *Nicotiana benthamiana* plants. After culturing for 3 days, the localization of GFP protein was observed using an LSM 710 laser confocal microscope (Carl Zeiss, Jena, Germany).

2.8. Yeast One-Hybrid Assay and Luciferase Complementation Assay (LUC)

To investigate the regulatory relationship, the CDS of *JrBBX3* was cloned into pGADT7, while the promoter of *JrUFGT5* was inserted into pABAi. The pro*JrUFGT5*-pABAi was transformed into yeast strain Y1HGold using a Matchmaker™ Gold Yeast One-Hybrid Library Screening System Kit (Clontech, San Francisco, CA, USA) and was cultured on SD/-Ura medium with an optimal concentration of AbA (Aureobasidin A, Coolaber, Beijing, China). Then, *JrBBX3*-pGADT7 was transformed into the Y1HGold competent cell with pro*JrUFGT5*-pABAi. Plates were incubated on SD/-Ura medium at 28 °C for 3–5 days before observation and photography [48].

To further test the regulation of JrBBX3 to *JrUFGT5*, the promoter sequence of *JrUFGT5* was cloned into pGreenII0800-LUC, while the CDS sequence of *JrBBX3* was cloned into the pSAK277 vector. The recombinant vectors were transformed into *Agrobacterium tumefaciens* strain GV3101, and resuspended in a MES suspension solution (B&M, Beijing, China) to OD_{600} = 0.6–0.8. After culturing in the dark for 3 h, the resuspended solution was injected into the leaves of four-week-old *Nicotiana benthamiana* plants. The tobacco leaves were used to test the LUC and REN activity after 24 h dark and 24 h light training [48].

2.9. Functional Analysis of JrBBX3

To investigate the function of *JrBBX3* in anthocyanin biosynthesis, the *JrBBX3-SAK Agrobacterium* suspension was resuspended in MES solution (B&M, Beijing, China) (adjusted to OD_{600} = 0.8) for infiltration into young red walnut leaves. Vacuum infiltration was performed at 0.085 MPa for 45 min. The infiltrated leaves were incubated in darkness for 24 h, followed by 48 h light exposure. RNA was subsequently extracted from the treated leaves for qRT-PCR analysis.

Approximately 0.1 g of treated leaf tissue was supplemented with a 1% hydrochloric acid–methanol solution (SCR, Shanghai, China), incubated for 24 h, and centrifuged at 12,000 rpm for 10 min at 4 °C to collect the supernatant. Absorbance values were measured at wavelengths of 530 nm, 620 nm, and 650 nm. The total anthocyanin content (mg per g of fresh weight) was calculated using the following formula:

$[(A_{530} - A_{620}) - 0.25(A_{650} - A_{620})]/0.1$. Three biological replicates were performed for each sample [49].

2.10. Statistical Analysis

All experimental data presented in this study represent the mean values ± SD, derived from a minimum of three independent biological replicates obtained from separate experimental cycles using distinct sample batches. Intergroup comparisons were assessed via one-way ANOVA with significance thresholds defined as follows: * $p < 0.05$ (statistical significance), ** $p < 0.01$ (high statistical significance), and ns $p \geq 0.05$ (non-significant results). These analyses were performed with the SPSS 18.0 software.

3. Results

3.1. Characterization of BBX Genes in Juglans Regia

A total of 39 *BBX* genes were identified from the walnut genome and renamed as *JrBBX1* to *JrBBX39* according to the physical positions on each chromosome. The 39 *JrBBX* genes were unevenly distributed on 14 of the 16 chromosomes: the largest number of *JrBBX* genes was six on Chr 3, while only one *JrBBX* was located on Chr2, Chr 9, Chr 12 and Chr 16, and no *JrBBX* was located on Chr 13 and 14. In the figure, red and blue indicate high and low density, respectively (Figure 1).

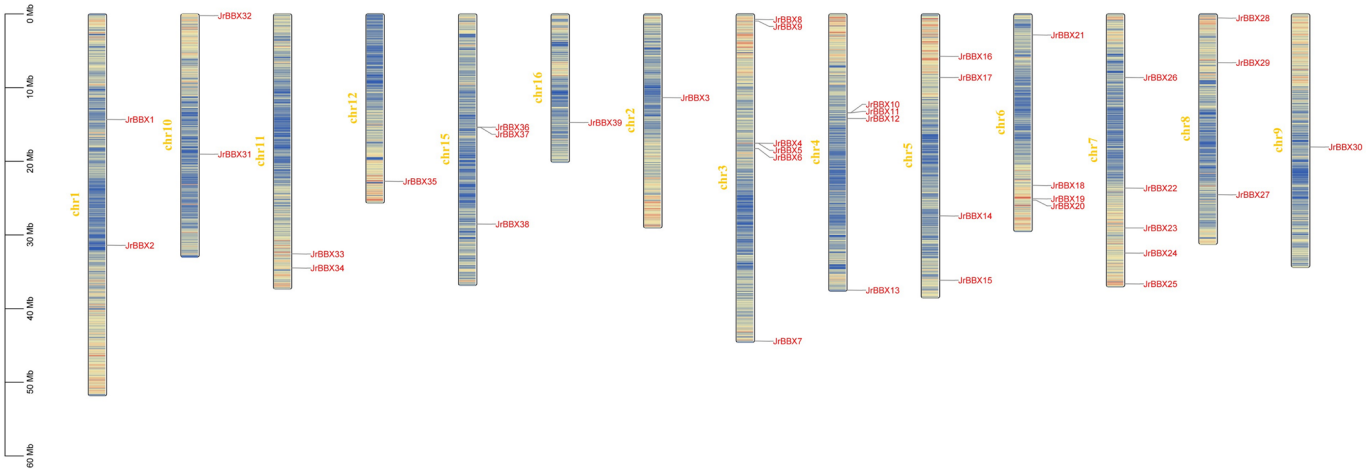

Figure 1. Location of *JrBBX* genes on walnut chromosomes. Chr1-Chr16 indicates the 16 chromosomes. Gene positions and chromosome length were measured using the scale on the left in mega bases (bp). Red and blue indicate high and low density, respectively.

The physicochemical properties of JrBBXs are shown in Table S4. The length of the CDS of *JrBBX* genes ranged from 387 bp (*JrBBX11*) to 1611 bp (*JrBBX26*), and the corresponding protein sequence length ranged from 128 to 536. The molecular weight (MW) was between 14.137 kDa (JrBBX11) and 59.874 kDa (JrBBX26). The theoretical isoelectric point (pI) ranged from 4 (JrBBX30) to 9.01 (JrBBX37). Additionally, the subcellular localization prediction showed that the majority of JrBBX members were localized in the nucleus, chloroplast and cytoplasm, respectively.

3.2. Phylogenetic and Gene Structure Analyses of the JrBBX Genes

A physical tree was constructed from the protein sequences of JrBBXs, AtBBXs and the BBXs associated with anthocyanin biosynthesis from other species. The results showed that all analyzed BBX proteins clustered into six distinct classes. Among the JrBBX proteins, class V contained the largest number (twelve), while classes VI contained only two

(Figure 2). Notably, the BBXs related to anthocyanin biosynthesis were predominantly concentrated in class V, except for VvBBX44 in class II.

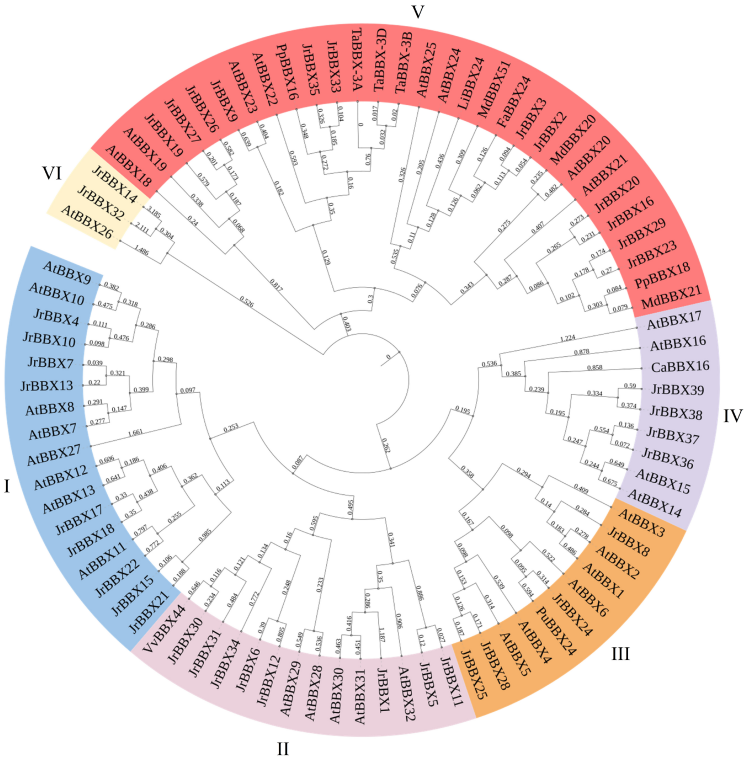

Figure 2. Phylogenetic analysis of BBX proteins between different species. Phylogenetic tree constructed with the BBXs of walnut, *Arabidopsis thaliana* and proteins related to anthocyanin biosynthesis in other species. Blue represents the class I, pink the class II, orange the class III, purple the class IV, red the class V, and yellow the class VI. Branch length represents phylogenetic relationship; different colors indicate distinct subfamilies. The accession numbers of the BBXs related to anthocyanin biosynthesis are as follows: *Lagerstroemia indica* LiBBX24 (WKZ09233.1), *Fragaria* × *ananassa* FaBBX24 (WMZ41122.1), *Triticum aestivum* TaBBX-3A (KAF7021760.1), *Triticum aestivum* TaBBX-3B (KAF7028614.1), *Triticum aestivum* TaBBX-3D (KAF7035694.1), *Malus domestica* MdBBX51 (MD17G1243400), *Malus domestica* MdBBX20 (MD10G1066000), *Malus domestica* MdBBX21 (MD08G1021000), *Vitis vinifera* VvBBX44 (CAN67068.1), *Pyrus communis* PpBBX16 (XP_068338627.1), and *Pyrus communis* PpBBX18 (XP_068314016.1).

To further analyze the structural composition of the JrBBX family, the JrBBX proteins were identified as conserved protein motifs by NCBI-CDD. Along with the physical tree, the JrBBXs were divided into six classes. Class I members exclusively contain two BBX domains. Class II features two BBX domains and one CCT domain; Class III possesses one BBX domain and one CCT domain. Class IV has a single BBX domain, and Class V members, despite sharing identical domain architecture with Class II (two BBX domains and one CCT domain), exhibit a distant phylogenetic relationship based on comparative analysis. Furthermore, JrBBX14 and JrBBX32 contained one BBX domain and one PLATZ domain (Figure S1a). The MEME server was used to identify the conserved motif of JrBBX proteins; ten conserved motifs were identified. The most closely related members had a common motif composition, and the protein-conserved motifs of JrBBXs ranged from 3 to 10 (Figure S1b). For gene structure, there are significant differences in the numbers of exons and introns. Among them, *JrBBX5*, *JrBBX11*, *JrBBX1*, *JrBBX30*, and *JrBBX31* in class IV had no introns, and the largest number of introns was 11 in *JrBBX26* (Figure S1c).

Prediction of the secondary structures of JrBBX proteins showed that all members contained α-helices, extended strands, β-turns, and random coils. Among them, the

proportion of α-helices ranged from 13.53% (JrBBX31) to 42.86% (JrBBX1), extended strands from 7.14% (JrBBX1) to 26.48% (JrBBX14), β-turns from 1.10% (JrBBX22) to 8.82% (JrBBX31), and random coils from 37.53% (JrBBX14) to 69.28% (JrBBX16) (Figure S1). To further understand the function of JrBBX proteins, the three-dimensional (3D) structures were predicted using SWISS-MODEL. The results showed that 39 JrBBX proteins were mainly composed of α-helices and random coils. According to protein sequence alignment, JrBBX domains located in random coils (Figure S2).

3.3. Collinear Analysis of JrBBXs

To further analyze the origins and evolutionary relationships of JrBBXs, the intra- and interspecific collinearity were assessed. The results showed that 26 segmental duplicated BBX gene pairs were discovered in the *J. regia* genome (Figure 3A and Table S5). Additionally, there were collinearity relationships between *J. regia* and *A. thaliana*/*J. sigillata*. Homologous *BBX* genes were shown to be scattered across various chromosomes with 39 collinear gene pairs with *A. thaliana*, and 76 collinear gene pairs between *J. regia* and *J. sigillata* (Figure 3B and Table S5). Comparative analysis of the BBX family with other species provided a research reference for analyzing the genetic relationships and gene functions of species.

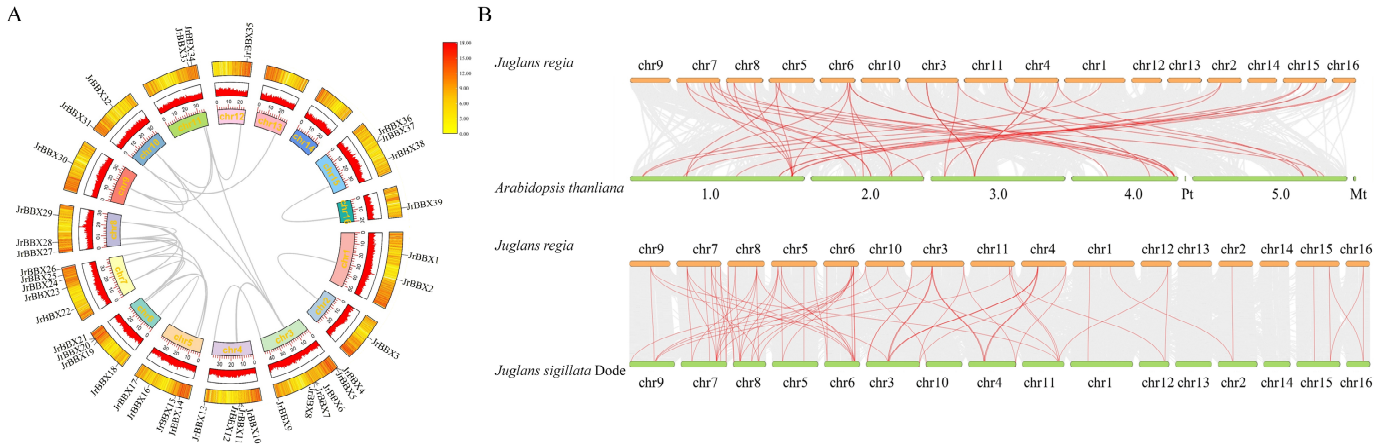

Figure 3. Intra- and interspecific collinearity analysis of *JrBBX* genes. (**A**): Intraspecific collinearity assessment of the *JrBBXs*, with red lines denoting homologous relationships among *JrBBX* genes and gray lines illustrating homology blocks across the *J. regia* genome. (**B**): Interspecific collinearity analysis of *J. regia* with *A. thaliana* and *J. sigillata*. Gray lines depict colinear regions between *J. regia* and other plant genomes, while red lines specifically highlight homologous gene pairs within the BBX family.

3.4. Prediction of Cis-Acting Elements of JrBBX Family Members

The 2000 bp upstream sequence of each *JrBBX* gene was used to analyze the *cis*-acting elements. As shown in Figure S3 and Table S6, light responsiveness elements, hormone response elements (including ABA, MeJA, auxin, gibberellin, ethylene and SA), transcription factor binding sites, wound responsiveness elements, defense and stress responsiveness elements were detected. All the members contained light responsiveness elements, among which *JrBBX1* possessed up to 23 light responsiveness elements, and *JrBBX37* only contained two. For hormone responsiveness elements, all *JrBBXs* except *JrBBX14* contained ABA responsiveness elements, ranging from one (*JrBBX8*, *JrBBX16*, *JrBBX29*, *JrBBX36* and *JrBBX39*) to ten (*JrBBX19*). *JrBBX9* and *JrBBX25* contained three auxin responsiveness elements, *JrBBX28* contained twelve ethylene responsiveness elements, JrBBX11 contained three gibberellin responsiveness elements, *JrBBX17* contained seventeen MeJA responsiveness elements, and *JrBBX22* contained four SA responsiveness elements,

which were the highest in *JrBBXs*, respectively. All members except *JrBBX18* contained MYB binding sites from one (*JrBBX19*) to eleven (*JrBBX30*), and all members except *JrBBX1* contained MYC binding sites from one (*JrBBX7*, *JrBBX12*, *JrBBX27*, *JrBBX34* and *JrBBX35*) to ten (*JrBBX38*). These results suggested that different *JrBBXs* might be related to various biological functions in walnut.

3.5. Protein–Protein Interaction in JrBBXs

The roles of JrBBXs during potential interactions were created by the STRING database (Figure S4). JrBBX39, JrBBX2/3, JrBBX6/12, JrBBX30/31/34, JrBBX5/11, JrBBX9/33, JrBBX36/37/38, JrBBX24 and JrBBX19/27 showed extensive interactions with the majority of JrBBX proteins, suggesting major functions in the BBX PPI network.

3.6. Expression Characteristic of JrBBX Genes in Different Walnut Colored Seed Coats

The expression pattern of all *JrBBX* genes in different colored seed coats was analyzed using the transcription sequencing data obtained from the seed coats of 'Zhonglin 1' and 'RW-1' at the S2 stage. *JrBBXs* showed distinct expression patterns in different colored seed coats. Among them, eight differentially expressed *JrBBXs* in 'Zhonglin 1' and 'RW-1' at the S2 stage were identified, with five upregulated and three downregulated (Figure 4A). To further investigate the correlation between *JrBBXs* expression and anthocyanin accumulation during seed coat development, the eight DEGs were selected for qRT-PCR validation across multiple developmental stages (S1–S3). Compared with that in 'Zhonglin 1', the expression of *JrBBX1* in 'RW-1' was upregulated only in S2, *JrBBX2* was upregulated in S2 and downregulated in S1 and S3, *JrBBX3* was downregulated in S1 and S2, *JrBBX5* and *JrBBX24* were downregulated in S1 and S3, *JrBBX15* was downregulated in S1 and upregulated in S3, *JrBBX23* was downregulated in S1 and upregulated in S2, and *JrBBX32* was upregulated in S1 and S2 while being downregulated in S3 (Figure 4B). Combining the results of phylogenetic tree results, JrBBX3 exhibited a close phylogenetic relationship with positive anthocyanin biosynthesis regulators MdBBX51 and FaBBX24. Given its low expression level in the 'RW-1' seed coat, JrBBX3 was selected out as the negative regulator in anthocyanin biosynthesis.

3.7. Subcellular Location of JrBBX3

In order to explore the location of JrBBX3 in cells, the CDS sequence of *JrBBX3* was cloned into pCAMBIA2300-GFP to obtain the recombinant vector JrBBX3-GFP. After *Agrobacterium*-mediated transformation into GV3101, the transient expression experiment in *N. benthamiana* leaves was performed (Figure 5). Confocal microscopy observation displayed the green fluorescence signal of JrBBX3-GFP protein at both cytoplasmic and nuclear locations. The result suggested that beside putative role in transcriptional regulation, JrBBX3 may also undergo nucleocytoplasmic shuttling to fine-tune its regulatory activity.

3.8. JrBBX3 Negatively Regulates the Expression of JrUFGT5

To investigate the role of JrBBX3 in anthocyanin biosynthesis regulation, the CDS of *JrBBX3* was cloned into the pGADT7 vector, while the promoter of the key anthocyanin biosynthetic gene *JrUFGT5* was cloned into the pABAi vector. The recombinant vector JrBBX3-AD was transformed into yeast Y1HGold with *ProJrUFGT5*-pABAi. The result suggested that JrBBX3 directly binds the *JrUFGT5* promoter (Figure 6A). Compared to the empty vector, JrBBX3 significantly suppressed the activity of *JrUFGT5* promoter (Figure 6B), with these results indicating that JrBBX3 acted as a negative regulator of *JrUFTG5*.

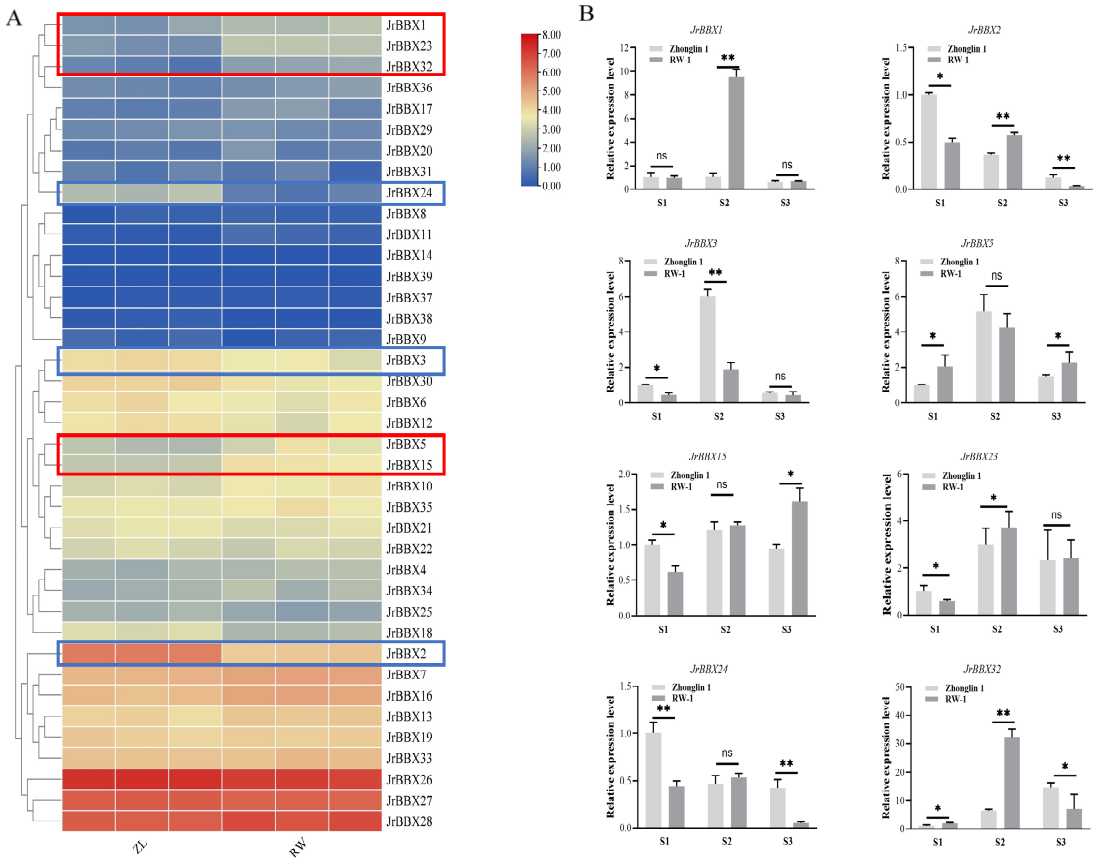

Figure 4. Expression profile of *JrBBX* genes. (**A**). The expression levels of 39 *JrBBX* genes in two walnut seed coats in S2. The red and blue bars (FPKM) indicate high and low expression, respectively. The red frame indicates the upregulated genes and the blue frame indicates the downregulated genes. (**B**). The relative expressions of 8 DEGs were detected by qRT-PCR. Seed coats of 'RW-1' and 'Zhonglin1' at different developmental stages: S1 (60 days after female flowering (DAF), hard stone stage), S2 (90 DAF, kernel filling stage), and S3 (120 DAF, kernel maturity stage). Significant differences were determined using a one-way ANOVA (ns $p > 0.05$, * $p < 0.05$, ** $p < 0.01$). Expression values (±SD) of three replicates were normalized using *Jr18S* as the internal control.

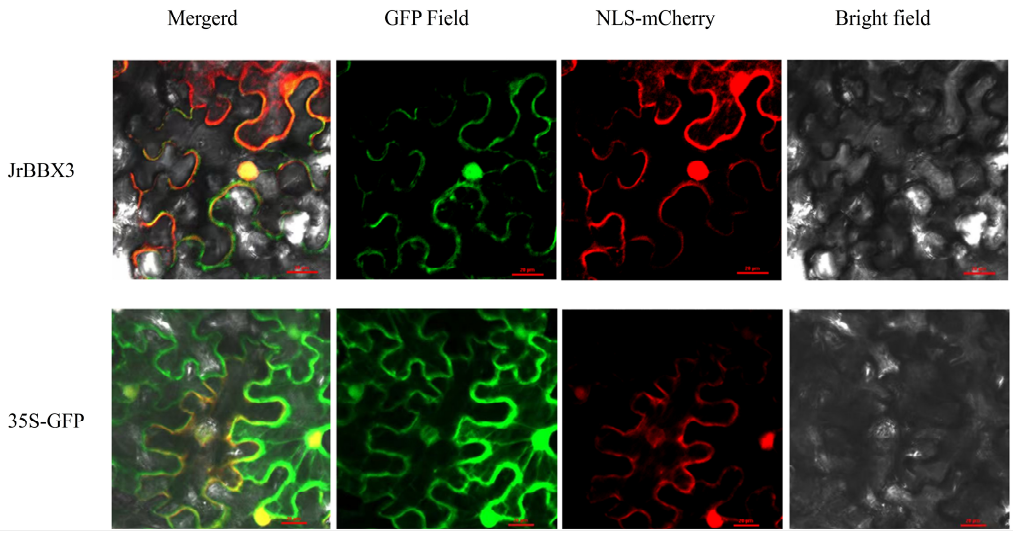

Figure 5. Subcellular localization of the JrBBX3 in *N. benthamiana* leaves. From left to right: Merged, GFP, mCherry, and bright-field; Bars = 20 μm.

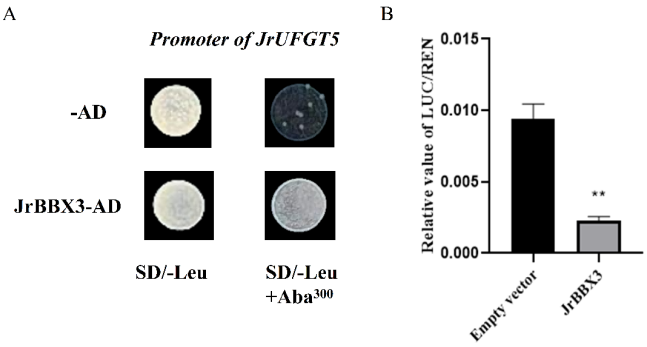

Figure 6. JrBBX3 binds to the promoter of *JrUFGT5*. (**A**) Y1H assay of JrBBX3 binding to the *JrUFGT5* promoter. The optimal Aba concentration to suppress basal promoter activity was 300 ng mL^{-1}. (**B**) Dual-luciferase assay of JrBBX3 regulation of *JrUFGT5* promoters, expressed as the ratio of LUC activity driven by the *JrUFGT5* promoter to the REN activity driven by the 35S promoter. ** $p \leq 0.05$.

3.9. JrBBX3 Negatively Regulates Anthocyanin Biosynthesis by Inhibiting the Expression of JrUFGT5

To investigate the function of JrBBX3 in anthocyanin biosynthesis, the *JrBBX3-SAK* vector was transformed into red walnut leaves to investigate the functions of anthocyanin biosynthesis using the *Agrobacterium* vacuum infiltration method. Overexpression of *JrBBX3* significantly inhibited red pigmentation compared with empty vector controls at 3 days post-transformation (Figure 7A). The *JrBBX3* expression level in overexpression treatment was significantly higher than in the control, while the expression of *JrUFGT5* significantly was downregulated (Figure 7B). Anthocyanin content decreased significantly in *JrBBX3* transformants (Figure 7C). These results demonstrate that JrBBX3 negatively regulates anthocyanin biosynthesis by inhibiting *JrUFGT5* expression.

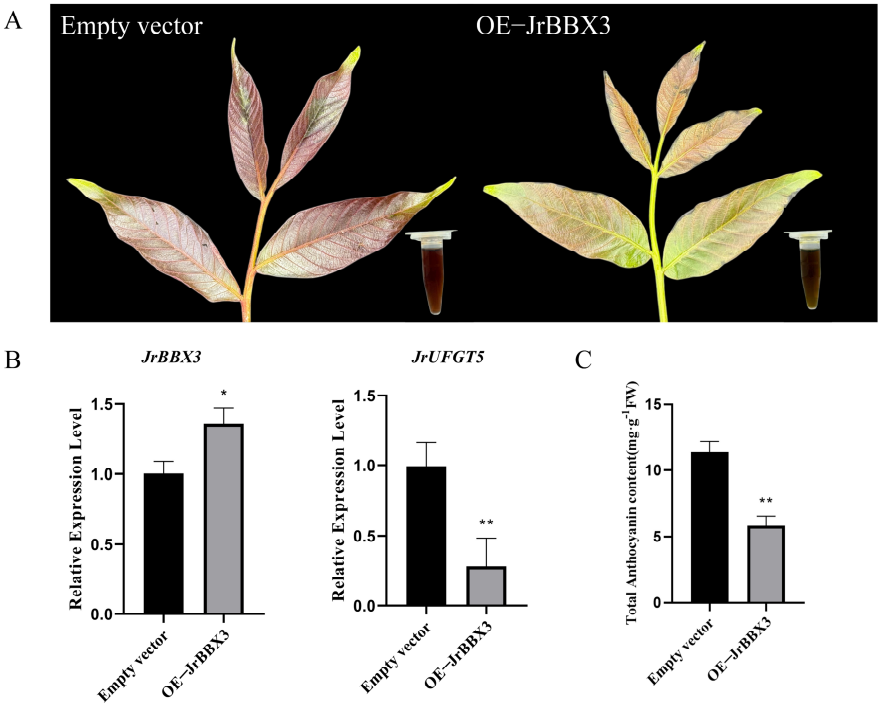

Figure 7. Overexpression of *JrBBX3* inhibited anthocyanin accumulation in walnut leaves. (**A**) Phenotypes of walnut leaves 3 days after transient transformation. (**B**) *JrBBX3* and *JrUFGT5* expression levels in walnut leaves 3 days after transient transformation. (**C**) Total anthocyanin content in walnut leaves 3 days after transient transformation. Data are means ± SD (n = 3). * $p \leq 0.05$, ** $p \leq 0.01$.

4. Discussion

Anthocyanin is an important type of secondary metabolite that enhances not only a plant's resistance, but also the nutritional value of its edible parts [49]. The BBX family, characterized by the BBX and CCT domains, exhibits functions in promoting or inhibiting anthocyanin biosynthesis. However, the BBX transcription factors involved in anthocyanin biosynthesis have not yet been reported in walnut. Here, 39 *JrBBX* genes were identified and screened from the walnut genome, which were unevenly distributed on 14 chromosomes. For comparison, previous studies have identified 24 BBX genes in the grape genome (*Vitis vinifera* L.) [50], 32 in Arabidopsis (*Arabidopsis thaliana* (L.) Heynh.) [38], 30 in rice (*Oryza sativa* L.) [51], and 37 in pear (*Pyrus bretschneideri* Rehd) [52], all of which are fewer than the number that were identified in walnut. In contrast, apple (*Malus domestica* Borkh) harbors 64 BBX genes [53], which is more than that in walnut. These results indicate that the number of *BBX* genes varies significantly among different plant species, which may be attributed to species-specific evolutionary processes, such as gene duplication, deletion, and divergence.

The *cis*-acting elements in the upstream promoter showed important roles in the functional diversity of genes [54]. Through PlantCARE analysis, light-responsive elements, hormone-responsive elements, stress-responsive elements, and transcription factor binding sites were enriched in the promoter of *JrBBXs*. Among these *cis*-acting elements, light-responsive elements were the most abundant, being identified in all JrBBX members. Light is well-documented to be vital for plant anthocyanin biosynthesis, as it modulates anthocyanin regulatory gene expressions [55,56]. Therefore, investigating whether light affects anthocyanin biosynthesis in red walnut will be the focus of our subsequent research. For hormone-responsive elements, all *JrBBXs* except the *JrBBX14* gene contained ABA responsiveness elements. In the previous study, ABA promoted anthocyanin biosynthesis in apple (*Malus domestica* Borkh) [57], Lycium (*Lycium ruthenicum* Murr.) [58], and litchi pericarp (*Litchi chinensis* Sonn.) [59]. Collectively, these findings suggest that both light and ABA treatment may regulate the expression of *JrBBX* genes, thereby participating in the regulation of anthocyanin biosynthesis in walnut. Furthermore, all members except *JrBBX18* contained MYB binding sites and all members except *JrBBX1* contained MYC binding sites, suggesting that *JrBBXs* were regulated by MYB and bHLH TFs, which are core components of the MBW complex—a key regulator of anthocyanin biosynthesis as mentioned earlier. The prediction results of protein–protein interactions showed that there are multiple interaction relationships among the members of the *JrBBX* gene family, which could further refine the regulatory network of anthocyanin biosynthesis in walnut.

The key JrBBXs in anthocyanin biosynthesis were selected using phylogenetic analysis, transcriptome sequencing and qRT-PCR. In comparison with the BBX protein in other species related to anthocyanin biosynthesis, twelve JrBBXs were divided into class V, representing those that may play roles in anthocyanin biosynthesis of walnut. This finding provides a theoretical basis for further functional characterization of JrBBXs in walnut anthocyanin accumulation. Transcriptome sequencing analysis revealed that eight *JrBBX* genes were differentially expressed between 'Zhonglin 1' and 'RW-1' with five being upregulated and three downregulated. Among them, JrBBX2 and JrBBX3 exhibited the highest homology with FaBBX24, a known positive regulator of anthocyanin biosynthesis in strawberry (*Fragaria* × *ananassa* Duch.) [60]. JrBBX23 showed high homology with MdBBX21 [61] and PpBBX18 [26], both of which are light-induced positive regulators of anthocyanin biosynthesis. Notably, all three JrBBX genes (*JrBBX2*, *JrBBX3*, and *JrBBX23*) belonged to Class V. To further validate the expression patterns of these key JrBBX genes, qRT-PCR analysis was performed, which indicated that *JrBBX3* was consistently downregulated during seed coat development; the other two genes (*JrBBX2* and *JrBBX23*) exhibited distinct

expression patterns. Based on these combined results, JrBBX3 was identified as a key BBX transcription factor involved in anthocyanin biosynthesis in the red walnut seed coat.

JrUFGT5, encoding anthocyanidin 3-*O*-glucosyltransferase, has previously been identified as a key structural gene associated with anthocyanin biosynthesis in walnut with higher expression [35]. Y1H and LUC assay results suggested that JrBBX3 negatively regulated the expression of *JrUFGT5*. Overexpression of *JrBBX3* in red walnut leaves was performed, and the treated leaves showed inhibited anthocyanin accumulation and *JrUFGT5* expression. Consistent with previous findings in Arabidopsis, AtBBX21, AtBBX22, and AtBBX23 acted as the positive regulators in anthocyanin biosynthesis [20–22]. Conversely, AtBBX24, AtBBX25 and AtBBX32 acted as repressors [23–25]. This finding establishes a direct negative regulatory relationship between JrBBX3 and anthocyanin biosynthesis.

5. Conclusions

In summary, this study systematically identified and analyzed the JrBBX gene family in red walnut (*Juglans regia* L. 'RW-1'), with the aim of elucidating its roles in anthocyanin biosynthesis. A total of 39 *JrBBX* genes (*JrBBX1-JrBBX39*) were identified from the walnut genome, which were unevenly distributed on 14 chromosomes. The phylogenetic analysis suggested that the JrBBXs are divided into six classes. *Cis*-acting element prediction showed that *JrBBXs* carried numerous light responsiveness elements, ABA responsiveness elements, MYB binding sites and MYC binding sites, suggesting the regulation of physiological processes by integrating light and ABA signals. The expression trends analysis revealed that eight *JrBBXs* were differently expressed in the 'Zhonglin 1' and 'RW-1' seed coat. qRT-PCR revealed that *JrBBX3* was downregulated in the red walnut seed coat. JrBBX3 localized at both the cytoplasm and nucleus and directly inhibited the activity of *JrUFGT5*, which is the key structural gene in anthocyanin biosynthesis. Conversely, overexpression of *JrBBX3* negatively regulated anthocyanin biosynthesis by inhibiting *JrUFGT5* expression. In conclusion, these results indicate that JrBBX3 contributed to the regulation of anthocyanin biosynthesis in red walnut through altering *JrUFGT5* expression. In this study, we provide important technical support and candidate genes for the genetic improvement of red walnut, which has important theoretical significance and practical application value.

Supplementary Materials: The following supporting information can be downloaded at https://www.mdpi.com/article/10.3390/horticulturae12050510/s1: Figure S1: The phylogenetic tree, predicted motifs and gene structure of JrBBXs; Figure S2: Secondary and tertiary structure prediction of JrBBX Proteins; Figure S3: Prediction of *cis*-acting elements in *JrBBX* gene family promoters (2000 bp). Figure S4: Prediction of the interaction network of JrBBX proteins. Table S1: The primers used in the study; Table S2: The accession numbers of AtBBXs; Table S3: The BBX protein sequences used in Figure 2. Table S4: Physicochemical properties of 39 JrBBX proteins in *J. regia*. Table S5: Homologous gene pairs within and between species of *J. regia*; Table S6: Prediction of *cis*-elements in *JrBBX* promoters.

Author Contributions: J.F., B.T. and L.W. conceived and designed the research. J.C., M.G. and S.T. carried out most of the experiments. X.W. and H.Z. performed the bioinformatics analyses. X.L. and N.H. analyzed the data. B.T. and L.W. wrote the paper. All authors have read and agreed to the published version of the manuscript.

Funding: This research was supported by funding from the National Natural Science Foundation of China (32301631), and the National Key R&D Program of China (2018YFD1000604).

Data Availability Statement: The data presented in this study are openly available in NCBI at [https://www.ncbi.nlm.nih.gov/bioproject/PRJNA1405992/] (accessed on 18 April 2026), reference number [PRJNA1405992].

Conflicts of Interest: The authors declare no conflicts of interest.

Abbreviations

The following abbreviations are used in this manuscript:

Aba	Aureobasidin A
ABA	Abscisic acid
CDS	Coding sequence
qRT-PCR	Quantitative real-time PCR
bp	Base pair
DEGs	Differentially expressed genes
AS	Acetosyringone
MES	2-Morpholinoethanesulfonic Acid
GFP	Green Fluorescent Protein
Y1H	Yeast One-Hybrid
LUC	Dual-luciferase assay
TFs	Transcription factors
CHS	Chalcone synthase
CHI	Chalcone isomerase
F3H	Flavanone 3-hydroxylase
F3′H	Flavonoid 3′-hydroxylase
F3′5′H	Flavonoid 3′5′-hydroxylase
DFR	Dihydroflavonol 4-reductase
ANS	Anthocyanidin synthase
UDFT	UDP-glucose: flavonoid-3-O-glucosyltransferase
CCT	CONSTANS, CO-LIKE and TOC1 motif
CAEs	*Cis*-acting elements
HMM	Hidden Markov Model

References

1. Castañeda-Ovando, A.; de Lourdes Pacheco-Hernández, M.; Páez-Hernández, M.E.; Rodríguez, J.A.; Galán-Vidal, C.A. Chemical studies of anthocyanins: A review. *Food Chem.* **2009**, *113*, 859–871. [CrossRef]
2. Jin, S.; Ye, N.; Chen, X.; Wang, P.; Gu, M.; Hou, B.; Zhang, C.; Zheng, Y.; Sun, Y. Identification of PAL genes related to anthocyanin synthesis in tea plants and its correlation with anthocyanin content. *Hortic. Plant J.* **2022**, *8*, 381–394. [CrossRef]
3. Zhao, X.C.; Zhang, Y.R.; Long, T.; Wang, S.C.; Yang, J. Regulation Mechanism of Plant Pigments Biosynthesis: Anthocyanins, Carotenoids, and Betalains. *Metabolites* **2022**, *12*, 871. [CrossRef]
4. Ma, Y.Y.; Ma, X.; Gao, X.; Wu, W.L.; Zhou, B. Light Induced Regulation Pathway of Anthocyanin Biosynthesis in Plants. *Int. J. Mol. Sci.* **2021**, *22*, 11116. [CrossRef] [PubMed]
5. Wu, T.; Liu, H.T.; Zhao, G.P.; Song, J.X.; Wang, X.L.; Yang, C.Q.; Zhai, R.; Wang, Z.G.; Ma, F.W.; Xu, L.F. Jasmonate and Ethylene-Regulated Ethylene Response Factor 22 Promotes Lanolin-Induced Anthocyanin Biosynthesis in 'Zaosu' Pear (*Pyrus bretschneideri* Rehd.) Fruit. *Biomolecules* **2020**, *10*, 278. [CrossRef] [PubMed]
6. Kenjiro, K.; Rintaro, S.; Wataru, T.; Noritoshi, I.; Toshimasa, Y.; Tomomi, H.; Yasuo, Y.; Toshiyuki, K.; Motoyuki, K.; Seiji, K.; et al. A new buckwheat dihydroflavonol 4-reductase (DFR), with a unique substrate binding structure, has altered substrate specificity. *BMC Plant Biol.* **2017**, *17*, 239. [CrossRef]
7. Lai, G.T.; He, L.Y.; Lin, J.X.; Guo, A.L.; Que, Q.X.; Che, J.M.; Guan, X.F.; Xiang, J.; Lai, C.C. Whole-pathway stimulation of anthocyanin biosynthesis by UDP-glycose: Flavonoid glycosyltransferase gene (UFGT) providing new insights into natural product development based on plant cell factory. *Food Biosci.* **2024**, *62*, 105409. [CrossRef]
8. Chen, L.; Hu, B.; Qin, Y.; Hu, G.; Zhao, J. Advance of the negative regulation of anthocyanin biosynthesis by MYB transcription factors. *Plant Physiol. Biochem.* **2019**, *136*, 178–187. [CrossRef]
9. LaFountain, A.M.; Yuan, Y.W. Repressors of anthocyanin biosynthesis. *New Phytol.* **2021**, *231*, 933–949. [CrossRef] [PubMed]
10. Ding, L.; Chen, X.; Wang, X.; Jiang, W.; Xu, X.; Hou, M.; Zhang, Y.; Wu, Z.; Chang, Y.; Xiang, Y. *ODR1*, the key seed dormancy and germination regulator, promotes seed Proanthocyanidin biosynthesis via interaction with TTG1 and modulation of MBW complex activity. *Plant J.* **2025**, *123*, e70434. [CrossRef]
11. Zhao, H.X.; Liu, L.S.; Chen, Y.; Li, C.L.; Wu, H.L.; Wang, T.; Shan, Z.; Wang, X.L.; Wu, Q. Transcription factors FtMYB22 negatively regulates anthocyanin synthesis by forming an MBW ternary complex in Tartary buckwheat. *Crop Sci.* **2024**, *64*, 853–869. [CrossRef]
12. Gangappa, S.N.; Botto, J.F. The BBX family of plant transcription factors. *Trends Plant Sci.* **2014**, *19*, 460–470. [CrossRef] [PubMed]

13. Heng, Y.; Jiang, Y.; Zhao, X.; Zhou, H.; Xu, D. BBX4, a phyB-interacting and modulated regulator, directly interacts with PIF3 to fine tune red light-mediated photomorphogenesis. *Proc. Natl. Acad. Sci. USA* **2019**, *116*, 26049–26056. [CrossRef]
14. Cao, J.; Yuan, J.; Zhang, Y.; Chen, C.; Zhang, B.; Shi, X.; Niu, R.; Lin, F. Multi-layered roles of BBX proteins in plant growth and development. *Stress Biol.* **2023**, *3*, 1. [CrossRef]
15. Yadav, A.; Ravindran, N.; Singh, D.; Rahul, P.; Datta, S. Role of Arabidopsis BBX proteins in light signaling. *J. Plant Biochem. Biotechnol.* **2020**, *29*, 623–635. [CrossRef]
16. Lin, F.; Jiang, Y.; Li, J.; Yang, T.T.; Fan, L.M.; Liang, J.S.; Xu, D.Q.; Chen, Z.J.; Deng, X.W. B-BOX DOMAIN PROTEIN28 Negatively Regulates Photomorphogenesis by Repressing the Activity of Transcription Factor HY5 and Undergoes COP1-Mediated Degradation. *Plant Cell* **2018**, *30*, 2006–2019. [CrossRef]
17. Bai, B.; Lu, N.N.; Li, Y.P.; Guo, S.L.; Yin, H.B.; He, Y.N.; Sun, W.; Li, W.; Xie, X.Z. OsBBX14 promotes photomorphogenesis in rice by activating OsHY5L1 expression under blue light conditions. *Plant Sci.* **2019**, *284*, 192–202. [CrossRef] [PubMed]
18. Chen, X.M.; Niu, M.Q.; Wu, X.P.; Peng, Y.K.; Zheng, R.Y.; Cheng, M.Y.; Zhao, K.; Zhou, Y.Z.; Peng, D.H. BBX Genes of Cymbidium ensifolium Exhibited Intense Response to Blue Light in Meristem Induction through Artificial Control. *Plants* **2024**, *13*, 2375. [CrossRef]
19. Yu, L.Y.; Wang, D.S.; Huang, R.M.; Cao, F.; Guo, C.L.; Zhang, J.Z. Genome-wide identification, characterization and expression profile analysis of BBX gene family in Chinese chestnut (*Castanea mollissima*). *Plant Biotechnol. Rep.* **2023**, *18*, 129–142. [CrossRef]
20. Xu, D.; Jiang, Y.; Li, J.; Lin, F.; Holm, M.; Deng, X.W. BBX21, an Arabidopsis B-box protein, directly activates HY5 and is targeted by COP1 for 26S proteasome-mediated degradation. *Proc. Natl. Acad. Sci. USA* **2016**, *113*, 7655–7660. [CrossRef]
21. Datta, S.; Johansson, H.; Hettiarachchi, C.; Irigoyen, M.L.; Desai, M.; Rubio, V.; Holm, M. LZF1/SALT TOLERANCE HOMOLOG3, an Arabidopsis B-box protein involved in light-dependent development and gene expression, undergoes COP1-mediated ubiquitination. *Plant Cell* **2008**, *20*, 2324–2338. [CrossRef]
22. Zhang, X.; Huai, J.; Shang, F.; Xu, G.; Tang, W.; Jing, Y.; Lin, R. A PIF1/PIF3-HY5-BBX23 transcription factor cascade affects photomorphogenesis. *Plant Physiol.* **2017**, *174*, 2487–2500. [CrossRef] [PubMed]
23. Job, N.; Yadukrishnan, P.; Bursch, K.; Datta, S.; Johansson, H. Two B-box proteins regulate photomorphogenesis by oppositely modulating HY5 through their diverse C-terminal domains. *Plant Physiol.* **2018**, *176*, 2963–2976. [CrossRef] [PubMed]
24. Gangappa, S.N.; Crocco, C.D.; Johansson, H.; Datta, S.; Hettiarachchi, C.; Holm, M.; Botto, J.F. The Arabidopsis B-BOX protein BBX25 interacts with HY5, negatively regulating BBX22 expression to suppress seedling photomorphogenesis. *Plant Cell* **2013**, *25*, 1243–1257. [CrossRef] [PubMed]
25. Holtan, H.E.; Bandong, S.; Marion, C.M.; Adam, L.; Tiwari, S.; Shen, Y.; Maloof, J.N.; Maszle, D.R.; Ohto, M.-A.; Preuss, S. BBX32, an Arabidopsis B-Box protein, functions in light signaling by suppressing HY5-regulated gene expression and interacting with STH2/BBX21. *Plant Physiol.* **2011**, *156*, 2109–2123. [CrossRef]
26. Bai, S.; Tao, R.; Yin, L.; Ni, J.; Yang, Q.; Yan, X.; Yang, F.; Guo, X.; Li, H.; Teng, Y. Two B-box proteins, PpBBX18 and PpBBX21, antagonistically regulate anthocyanin biosynthesis via competitive association with *Pyrus pyrifolia* ELONGATED HYPOCOTYL 5 in the peel of pear fruit. *Plant J.* **2019**, *100*, 1208–1223. [CrossRef]
27. Bai, S.; Tao, R.; Tang, Y.; Yin, L.; Ma, Y.; Ni, J.; Yan, X.; Yang, Q.; Wu, Z.; Zeng, Y. BBX16, a B-box protein, positively regulates light-induced anthocyanin accumulation by activating MYB10 in red pear. *Plant Biotechnol. J.* **2019**, *17*, 1985–1997. [CrossRef]
28. Yang, G.; Sun, M.; Brewer, L.; Tang, Z.; Nieuwenhuizen, N.; Cooney, J.; Xu, S.; Sheng, J.; Andre, C.; Xue, C. Allelic variation of BBX24 is a dominant determinant controlling red coloration and dwarfism in pear. *Plant Biotechnol. J.* **2024**, *22*, 1468–1490. [CrossRef]
29. An, J.-P.; Wang, X.-F.; Espley, R.V.; Lin-Wang, K.; Bi, S.-Q.; You, C.-X.; Hao, Y.-J. An apple B-Box protein MdBBX37 modulates anthocyanin biosynthesis and hypocotyl elongation synergistically with MdMYBs and MdHY5. *Plant Cell Physiol.* **2020**, *61*, 130–143. [CrossRef]
30. Qiu, Q.; Sun, Y.; Pagay, V.; Gao, J.; Zhou, M.; Hu, Y.; Wang, L.; Wang, S. VvBBX32 responds to high temperatures and mediates anthocyanin biosynthesis in 'Merlot'grape (*Vitis vinifera* L.) berries. *Plant Physiol. Biochem.* **2025**, *229*, 110275. [CrossRef]
31. Lei, F.M.; Liu, Y.Q.; Shi, T.M.; Zhang, L.F.; Zhang, Y.Q.; Song, L.J.; Huang, X.Q.; Li, N.; Li, M.J.; Shen, Y.; et al. Comprehensive Analysis in the Nutritional Composition, Bioactive Contents, and Antioxidant Capacity of Walnut (*Juglans regia* L.) Male Flowers. *Foods* **2025**, *14*, 4250. [CrossRef]
32. Njike, V.Y.; Costales, V.C.; Petraro, P.; Annam, R.; Yarandi, N.; Katz, D.L. The Resulting Variation in Nutrient Intake With the Inclusion of Walnuts in the Diets of Adults at Risk for Type 2 Diabetes: A Randomized, Controlled, Crossover Trial. *Am. J. Health Promot.* **2019**, *33*, 430–438. [CrossRef]
33. Li, Y.Z.; Luo, X.; Wu, C.Y.; Cao, S.Y.; Zhou, Y.F.; Jie, B.; Cao, Y.L.; Meng, H.J.; Wu, G.L. Comparative Transcriptome Analysis of Genes Involved in Anthocyanin Biosynthesis in Red and Green Walnut (*Juglans regia* L.). *Molecules* **2017**, *23*, 25. [CrossRef] [PubMed]

34. Wang, L.; Li, L.; Zhao, W.; Fan, L.; Meng, H.; Zhang, G.; Wu, W.; Shi, J.; Wu, G. Integrated metabolomic and transcriptomic analysis of the anthocyanin and proanthocyanidin regulatory networks in red walnut natural hybrid progeny leaves. *PeerJ* **2022**, *10*, e14262. [CrossRef] [PubMed]
35. Zhao, W.; Fan, L.; Wu, W.; Li, Y.; Meng, H.; Wang, G.; Dong, Z.; Wang, L.; Wu, G. Re-sequencing and transcriptomic analysis reveal differential expression patterns and sequence variation in glucosyltransferase gene related to anthocyanin biosynthesis in walnut (*Juglans regia* L.). *Sci. Hortic.* **2023**, *317*, 112077. [CrossRef]
36. Zhao, W.; Liu, Y.; Li, L.; Meng, H.; Yang, Y.; Dong, Z.; Wang, L.; Wu, G. Genome-wide identification and characterization of bHLH transcription factors related to anthocyanin biosynthesis in red walnut (*Juglans regia* L.). *Front. Genet.* **2021**, *12*, 632509. [CrossRef]
37. Zhang, J.; Zhang, W.; Ji, F.; Qiu, J.; Song, X.; Bu, D.; Pan, G.; Ma, Q.; Chen, J.; Huang, R. A high-quality walnut genome assembly reveals extensive gene expression divergences after whole-genome duplication. *Plant Biotechnol. J.* **2020**, *18*, 1848. [CrossRef]
38. Khanna, R.; Kronmiller, B.; Maszle, D.R.; Coupland, G.; Holm, M.; Mizuno, T.; Wu, S.-H. The Arabidopsis B-box zinc finger family. *Plant Cell* **2009**, *21*, 3416–3420. [CrossRef]
39. Finn, R.D.; Bateman, A.; Clements, J.; Coggill, P.; Eberhardt, R.Y.; Eddy, S.R.; Heger, A.; Hetherington, K.; Holm, L.; Mistry, J.; et al. Pfam: The protein families database. *Nucleic Acids Res.* **2014**, *42*, 222–230. [CrossRef]
40. Azimi, R.; Ozgul, M.; Kenney, M.C.; Kuppermann, B.D. Bioinformatic Analysis of Small Humanin Like Peptides using AlfaFold-2 and Expasy ProtParam. *Investig. Ophthalmol. Vis. Sci.* **2024**, *65*, 1320.
41. Dong, X.B.; Ding, C.Q.; Zhang, X.N.; Lei, L.; Chen, Y.; Fu, Q.Y.; Yang, Y.; Hao, Y.W.; Ye, M.; Zeng, J.M.; et al. Analysis of the two-component system gene family and the positive role of CsRR5 in cold stress response in tea plants. *Plant Physiol. Biochem.* **2025**, *222*, 109739. [CrossRef]
42. Yuan, S.; Chan, H.S.; Hu, Z. Using PyMOL as a platform for computational drug design. *Wiley Interdiscip. Rev. Comput. Mol. Sci.* **2017**, *7*, e1298. [CrossRef]
43. Wang, Z.; Cui, R.; Gao, J.; Jia, L.; Yan, C.; Shu, Y.; Zhang, K. Genome-wide identification, stress-responsive expression analysis, and key candidate gene mining of the SAP gene family in cucumber and watermelon. *Sci. Hortic.* **2025**, *353*, 114475. [CrossRef]
44. Xu, Y.; Zhang, Y.; Li, C.Z.; Yin, R.X.; Lin, H.; Zuo, Y.; Huang, X.; Qin, B.; Ju, Y.Q. Genome-wide characterization of the TCP family in Lagerstroemia and functional analysis of LfiTCP12 uncover its role in shoot branching promotion. *Plant Cell Rep.* **2026**, *45*, 108. [CrossRef] [PubMed]
45. Tong, C.; Jia, Y.; Hu, H.F.; Zeng, Z.H.; Brett, C.; Li, C.D. Pangenome and pantranscriptome as the new reference for gene-family characterization: A case study of basic helix-loop-helix (bHLH) genes in barley. *Plant Commun.* **2025**, *6*, 101190. [CrossRef]
46. Zhang, M.L.; Zhu, F.; Sun, G.; Mi, Y.J.; Zhang, X.K.; Zhao, S.F.; Yu, Y.; Xi, H. The Analysis of the Glycosyltransferase Activity Gene Family in Gossypium hirsutum and Functional Verification of GTs Conferring Resistance to *Verticillium* Wilt. *Int. J. Mol. Sci.* **2025**, *26*, 3170. [CrossRef]
47. Siddique, M.N.A.; Jone, M.J.H.; Naher, J.; Hossain, M.R. Genome-wide identification and expression analysis of the trihelix gene family in melon. *Heliyon* **2026**, *12*, e44714. [CrossRef]
48. Lan, Y.H.; Gong, F.Y.; Dong, R.J.; Li, C.; Xia, F.; Li, Y.F.; Liu, X.J.; Liu, D.C.; Liang, G.Y.; Fang, C.; et al. A R2R3-MYB transcription factor SmMYB88 of Solanum melongena regulates cold tolerance by activating antioxidant system. *Plant Cell Rep.* **2026**, *45*, 28. [CrossRef]
49. Jian, W.; Ou, X.; Sun, L.; Chen, Y.; Liu, S.; Lu, W.; Yang, X.; Zhao, Z.; Li, Z. Characterization of anthocyanin accumulation, nutritional properties, and postharvest attributes of transgenic purple tomato. *Food Chem.* **2023**, *408*, 135181. [CrossRef]
50. Wei, H.; Wang, P.; Chen, J.; Li, C.; Wang, Y.; Yuan, Y.; Fang, J.; Leng, X. Genome-wide identification and analysis of B-BOX gene family in grapevine reveal its potential functions in berry development. *BMC Plant Biol.* **2020**, *20*, 72. [CrossRef]
51. Huang, J.; Zhao, X.; Weng, X.; Wang, L.; Xie, W. The rice B-box zinc finger gene family: Genomic identification, characterization, expression profiling and diurnal analysis. *PLoS ONE* **2012**, *7*, e48242. [CrossRef] [PubMed]
52. Zou, Z.; Wang, R.; Wang, R.; Yang, S.; Yang, Y. Genome-wide identification, phylogenetic analysis, and expression profiling of the BBX family genes in pear. *J. Hortic. Sci. Biotechnol.* **2018**, *93*, 37–50. [CrossRef]
53. Liu, X.; Li, R.; Dai, Y.; Chen, X.; Wang, X. Genome-wide identification and expression analysis of the B-box gene family in the Apple (*Malus domestica* Borkh.) genome. *Mol. Genet. Genom.* **2018**, *293*, 303–315. [CrossRef] [PubMed]
54. Wittkopp, P.J.; Kalay, G. Cis-regulatory elements: Molecular mechanisms and evolutionary processes underlying divergence. *Nat. Rev. Genet.* **2012**, *13*, 59–69. [CrossRef]
55. Caid, M.B.E.; Lachheb, M.; Lagram, K.; Wang, X.K.; Serghini, M.A. Ecotypic variation and environmental influence on saffron (*Crocus sativus* L.) vegetative growth: A multivariate performance analysis. *J. Appl. Res. Med. Aromat. Plants* **2024**, *43*, 100601. [CrossRef]
56. Mohamed, B.E.C.; Latifa, S.; Soumaya, E.M.; Khadija, L.; Khalid, L.; Abdelhamid, E.M.; Amine, S.M. Multi-site evaluation of the productivity among saffron (*Crocus sativus* L.) for clonal selection purposes. *J. Appl. Res. Med. Aromat. Plants* **2020**, *17*, 100248. [CrossRef]

57. An, J.-P.; Zhang, X.-W.; Liu, Y.-J.; Wang, X.-F.; You, C.-X.; Hao, Y.-J. ABI5 regulates ABA-induced anthocyanin biosynthesis by modulating the MYB1-bHLH3 complex in apple. *J. Exp. Bot.* **2021**, *72*, 1460–1472. [CrossRef]
58. Li, G.; Zhao, J.; Qin, B.; Yin, Y.; An, W.; Mu, Z.; Cao, Y. ABA mediates development-dependent anthocyanin biosynthesis and fruit coloration in Lycium plants. *BMC Plant Biol.* **2019**, *19*, 317. [CrossRef]
59. Wei, Y.-Z.; Hu, F.-C.; Hu, G.-B.; Li, X.-J.; Huang, X.-M.; Wang, H.-C. Differential expression of anthocyanin biosynthetic genes in relation to anthocyanin accumulation in the pericarp of Litchi chinensis Sonn. *PLoS ONE* **2011**, *6*, e19455. [CrossRef]
60. Zhang, L.; Wang, Y.; Yue, M.; Jiang, L.; Zhang, N.; Luo, Y.; Chen, Q.; Zhang, Y.; Wang, Y.; Li, M. FaMYB5 interacts with FaBBX24 to regulate anthocyanin and proanthocyanidin biosynthesis in strawberry (*Fragaria× ananassa*). *Int. J. Mol. Sci.* **2023**, *24*, 12185. [CrossRef]
61. Zhang, B.; Zhu, Z.-Z.; Qu, D.; Wang, B.-C.; Hao, N.-N.; Yang, Y.-Z.; Yang, H.-J.; Zhao, Z.-Y. MdBBX21, a B-box protein, positively regulates light-induced anthocyanin accumulation in apple peel. *Front. Plant Sci.* **2021**, *12*, 774446. [CrossRef] [PubMed]

Disclaimer/Publisher's Note: The statements, opinions and data contained in all publications are solely those of the individual author(s) and contributor(s) and not of MDPI and/or the editor(s). MDPI and/or the editor(s) disclaim responsibility for any injury to people or property resulting from any ideas, methods, instructions or products referred to in the content.